Control allocation for optimal and resilient operation of the MMC

Grégoire Le Goff, Marc Bodson, Maurice Fadel

Control allocation for optimal and resilient operation of the MMC

Grégoire Le Goff
LAPLACE
University of Toulouse, CNRS, INPT
Toulouse, France
legoff@laplace.univ-tlse.fr

Marc Bodson
Dept. of Electrical and Computer Engineering
University of Utah, Salt Lake City
Utah, USA
bodson@eng.utah.edu

Maurice Fadel
LAPLACE
University of Toulouse, CNRS, INPT
Toulouse, France
fadel@laplace.univ-tlse.fr

***Abstract*—The article proposes a new approach to modular multilevel converter (MMC) control. A key feature is the use of real-time optimization for arm voltage regulation and for balancing of the capacitor voltages in the submodules (SMs). The control allocation (CA) method automatically and optimally distributes the control requirements among a large number of switches. As a benefit, the algorithm can be adapted with almost no modification to accommodate failures. First, a control-oriented approach is used to derive the necessary models. Then, the MMC control architecture is designed. Simulations demonstrate the effectiveness of the approach on an MMC with 50 SMs per arm. Test cases include steady state and transient conditions, as well as operation without and with multiple SM faults.**

***Index Terms*—MMC, Control Allocation, Fault Tolerant Control, Real-Time Optimization, Submodule faults**

I. Introduction

A. Interest in versatile, flexible and resilient grids

The last decade has seen the growing development of renewable energy sources and their increasing share of the grid [1], [2]. However, the renewable sources producing this electrical energy are fluctuating over time. As a result, the grid must be able to adapt to this variable energy supply while meeting the power demand. Thus, challenges have arisen in the aim of having a versatile, flexible, and reliable energy supply at the scale of the grid that meets the constraints imposed by the increasing share of renewables [2].

To achieve these objectives, a requirement lies in having reliable power conversion between components that transmit energy at various voltage levels. The MMC is increasingly used, as it has shown benefits compared to other multilevel DC-AC converters for medium-voltage (MV) and high-voltage (HV) power conversion (e.g. high efficiency, harmonic content quality, scalability to various power levels, wider power range capabilities, and simplified manufacturing). Addressing fault tolerant control for the MMC is a challenging topic [3] that requires dedicated control approaches accounting for the topological specificities of such converters.

B. Objectives of the research work

This paper contributes to an overall research objective aimed at developing novel control allocation methods for the MMC [4], [5]. The goal is to optimize the converter control in real time, taking full advantage of the large number of SMs, and to operate as effectively as possible, whether in healthy or faulty mode.

C. Novelty of the proposed control approach

The voltages, currents, powers and the stored energies are all variables of interest for MMC control. For each of these quantities, a variety of control methods are available.

For voltages, most approaches involve two stages: the first stage determines the number of SMs to connect to the arm to get as close as possible to the arm voltage reference. The second stage selects the specific SMs to be included to ensure capacitor balancing [6]–[8]. Compared to these techniques, the major novelty of the approach proposed here is that the two objectives are addressed in a single and coordinated strategy using optimization. To generate a given arm voltage, the system with a large number of SMs is overactuated with constraints, and is suited to control allocation (CA) methods [9]–[11]. The capacitor voltages depend on the same control variables (duty cycles of the SMs). Balancing can be included in the optimization problem as a secondary objective.

Optimization methods have been applied to the MMC under the framework of model-predictive control (MPC) [12], [13]. Compared to these methods, CA features two main benefits: 1) the optimization is much faster, as it is performed with a prediction over a sampling period rather than a longer horizon, and 2) tuning of the closed-loop dynamics is considerably more straightforward.

In addition to the ability to address both voltage control objectives in a cooperative and optimized way, the other novelty of the approach is the capability of fault tolerant control (FTC) with the same algorithm. Two main families of SM fault-ridethrough solutions can be identified: 1) Structural modification of the MMC with modification of the SM topology or directly adding SMs in the arms, thus oversizing the MMC in nominal operation [8], [14], [15]; and 2) Reconfiguration of the control algorithm of the MMC. Some solutions may also be a mix of both families. The second family is the one to which the work presented here belongs. It can be organized in several categories starting with a) zero sequence voltage injection (ZSVI); b) capacitor voltage increment in the remaining healthy SMs; c) dedicated modulation techniques like selective harmonic elimination (SHE); d) modification of

the pulse-width modulation (PWM) carrier waveforms; or e) MPC algorithms that directly take into account fault-tolerant objectives in their optimization procedure to ensure the high-level current control stage [16]. More details about the above-mentioned approaches can be found in the review paper [17].

Unlike other techniques from the second family, the CA algorithm proposed here is able to immediately and optimally redistribute control effort to the remaining SMs as soon as a fault is detected, and without any modification to the code. This algorithm is directly implemented at the lower control level: the one in charge of voltage control.

For current control, a wide variety of controllers are available. Compared to conventional PI [6] or PR [18] controllers, the approach proposed here is a model-inversion based (MIB) CA method, which finds its effectiveness in the simple inversion of the current model. It can be likened to a state-feedback controller with additive non-linearity compensation. If integral action is desired, [19] explains how a transparent integral compensator can be added to CA methods without modification to the closed-loop dynamics.

The work presented here is a continuation of the research reported in [4], [5], [20]. In comparison, a different formulation of the optimization criterion is implemented, an improved circulating current injection method is used, and the fault-tolerant feature is tested.

D. Outline

The first part of the paper is dedicated to the control-oriented modeling of the MMC with the dynamic model of the currents, the energy, and the arm and capacitor voltages. Next, the control architecture implementing real-time optimization is presented with its various cascaded loops, each dedicated to one of the electrical quantities mentioned previously. The fourth section covers the simulation conditions and the associated results. The last section discusses conclusions that can be drawn from the paper.

II. Control-oriented modeling of the MMC

A. Introducting the MMC

The MMC is a multilevel converter consisting of elementary components called submodules (SMs) [7]. Generally speaking, SMs consist of one or several DC-DC converters along with a voltage source, as shown in Fig. 1 [21]. The most common types of SMs are the half-bridge (SM-HB) and the full-bridge (SM-FB) modules [22]. Each SM applies a given voltage level to the arm to which it belongs and is assumed to be controlled around a nominal voltage v_C^{nom}. Consequently, the stacks of SMs that comprise the arms are treated as continuously variable voltage sources. The overall arm voltages are the variables used to control the currents in the converter. The representation of the arm voltages is shown on Fig. 1 as v_{xy}. Note that x refers to the DC bus pole connection (p for positive and n for negative), and that y refers to the phase on the AC-side. Table I is given to establish the notation used in Fig. 1.

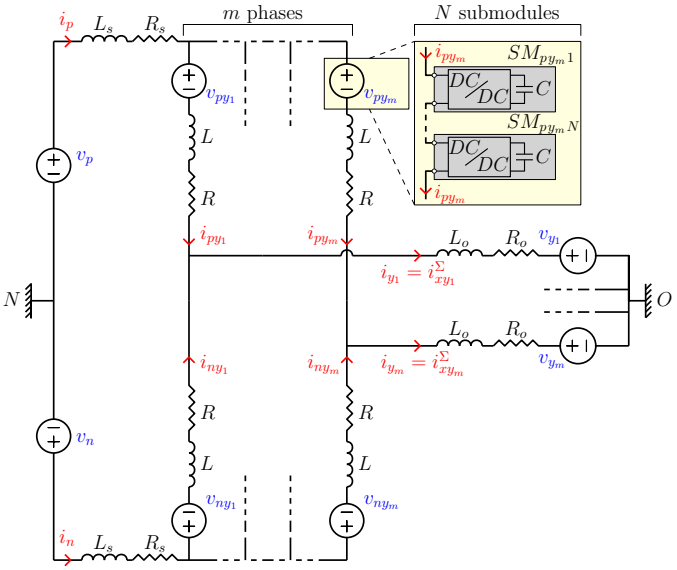

Fig. 1. Electrical diagram of the m-phase MMC.

TABLE I
MMC notation used in Fig. 1

Meaning	Symbol
DC-side poles	$x \in \{p, n\}$
Positive pole voltage and current	v_p and i_p
Negative pole voltage and current	v_n and i_n
DC-side voltage sum	$v_x^{\Sigma} = v_p + v_n$
DC bus voltage	$v_x^{\Delta} = v_p - v_n = V_{DC}$
DC-side current sum	$i_x^{\Sigma} = i_p + i_n$
DC-side current difference	$i_x^{\Delta} = i_p - i_n$
DC-side impedance	R_s, L_s
Arm voltage and current	v_{xy} and i_{xy}
Arm current sum	$i_{xy}^{\Sigma} = i_{py} + i_{ny} = i_y$
Arm current difference	$i_{xy}^{\Delta} = i_{py} - i_{ny}$
Switching frequency and period	f_s, T_s
Arm impedance	R, L
Number of phases	m
AC-side phases	$y \in \{y_1, \ldots, y_m\}$
AC-side voltage and current	v_y and $i_y = i_{xy}^{\Sigma}$
AC-side grid frequency and period	f_o, T_o
AC-side grid pulsation	$\omega_o = 2\pi f_o$
AC-side impedance	R_o, L_o
Zero sequence voltage	v_{NO}

B. Model of the currents

To develop the model of the currents, focus is on leg $\#y$ of the MMC shown in Fig. 1. Note that the derivative operator is replaced by the Laplace variable, s. Applying Kirchhoff's voltage law (KVL) on the current path flowing from the AC neutral point to the DC neutral point through the positive pole gives:

$$(\alpha_{py}) : v_y + (R_o + L_o s)\, i_{xy}^{\Sigma} + (R + Ls)\, i_{py} + v_{py} + (R_s + L_s s)\, i_p - v_p = v_{NO} \quad (1)$$

Applying the same law through the negative pole results in:

$$(\alpha_{ny}) : v_y + (R_o + L_o s)\, i_{xy}^{\Sigma} + (R + Ls)\, i_{ny} + v_{ny} + (R_s + L_s s)\, i_n - v_n = v_{NO} \quad (2)$$

From these equations, those describing the behavior from $i_y = i_{xy}^{\Sigma}$ and i_{xy}^{Δ} are now derived.

1) Dynamic behavior from i_{xy}^{Σ}: From (1) and (2), $(\alpha_{py}) + (\alpha_{ny})$ gives:

$$\begin{aligned} 2v_y + [(R+2R_o) + (L+2L_o)s]\, i_{xy}^{\Sigma} + (v_{py} + v_{ny}) \\ + (R_s + L_s s)\,(i_p + i_n) - (v_p + v_n) = 2v_{NO} \end{aligned} \tag{3}$$

KIRCHHOFF's current law (KCL), $i_p = \sum_y i_{py}$ and $i_n = \sum_y i_{ny}$ yields:

$$\begin{aligned} &[(R+2R_o) + (L+2L_o)s]\, i_{xy}^{\Sigma} + (R_s + L_s s) \textstyle\sum_y i_{xy}^{\Sigma} \\ &= -(v_{py} + v_{ny}) + v_x^{\Sigma} - 2v_y + 2v_{NO} \end{aligned} \tag{4}$$

This equation being valid $\forall y \in \{y_1, \ldots, y_m\}$, the m corresponding equations can be put in vector form:

$$\begin{aligned} &([(R+2R_o) + (L+2L_o)s]\, \mathbb{I}_m + (R_s + L_s s)\, \mathbb{J}_m)\ \mathbf{I^{\Sigma}} \\ &= -\begin{bmatrix} \mathbb{I}_m & \mathbb{I}_m \end{bmatrix} \mathbf{V_{xy}} + (v_x^{\Sigma} + 2v_{NO})\ \mathbf{n_{\Sigma}} - 2\mathbf{V_y} \end{aligned} \tag{5}$$

where $\mathbb{I}_m$ is the identity matrix of size m, $\mathbb{J}_m$ is a matrix of same size filled with 1's, $\mathbf{n_{\Sigma}} = [1\ \ldots\ 1]^T \in \mathbb{N}^m$, $\mathbf{I^{\Sigma}} \triangleq [i_{xy_1}^{\Sigma}\ \ldots\ i_{xy_m}^{\Sigma}]^T \in \mathbb{R}^m$, $\mathbf{V_{xy}} = [v_{py_1}\ \ldots\ v_{py_m}, v_{ny_1}\ \ldots\ v_{ny_m}]^T \in \mathbb{R}^{2m}$ and $\mathbf{V_y} = [v_{y_1}\ \ldots\ v_{y_m}]^T \in \mathbb{R}^m$. Note that, according to the direction of positive currents specified in Fig. 1, i_{xy}^{Σ} represents the current flowing towards the AC-side grid and contains the output AC currents as well as the common mode current.

2) Dynamic behavior from i_{xy}^{Δ}: From (1) and (2), $(\alpha_{py}) - (\alpha_{ny})$ gives:

$$\begin{aligned} (R+Ls)\, i_{xy}^{\Delta} + (v_{py} - v_{ny}) \\ + (R_s + L_s s)\,(i_p - i_n) - (v_p - v_n) = 0 \end{aligned} \tag{6}$$

With $i_p = \sum_y i_{py}$ and $i_n = \sum_y i_{ny}$, (6) is equivalent to:

$$(R+Ls)\, i_{xy}^{\Delta} + (v_{py} - v_{ny}) + (R_s + L_s s) \textstyle\sum_y i_{xy}^{\Delta} = -v_{xy}^{\Delta} + v_x^{\Delta} \tag{7}$$

This equation being valid $\forall y \in \{y_1, \ldots, y_m\}$, the m corresponding equations can be put in vector form, as was done to go from (4) to (5):

$$\begin{aligned} &[(R+Ls)\, \mathbb{I}_m + (R_s + L_s s)\, \mathbb{J}_m]\ \mathbf{I^{\Delta}} \\ &= -\begin{bmatrix} \mathbb{I}_m & -\mathbb{I}_m \end{bmatrix} \mathbf{V_{xy}} + v_x^{\Delta}\ \mathbf{n_{\Sigma}} \end{aligned} \tag{8}$$

with $\mathbf{I^{\Delta}} \triangleq [i_{xy_1}^{\Delta}\ \ldots\ i_{xy_m}^{\Delta}]^T \in \mathbb{R}^m$. Note that, according to the direction of positive currents specified in Fig. 1, i_{xy}^{Δ} contains the circulating current as well as the DC-side current supplying the MMC.

3) State-space model for all i_{xy}^{Σ} and i_{xy}^{Δ} currents: From (5) and (8), the combined state-space model of the currents is readily deduced:

$$\dot{\mathbf{I}}^{\mathbf{\Sigma\Delta}} = A_{\Sigma\Delta}\mathbf{I^{\Sigma\Delta}} + B_{\Sigma\Delta}\mathbf{V_{xy}} + \mathbf{E_{\Sigma\Delta}} \tag{9}$$

where:

$$\begin{aligned} \mathbf{I^{\Sigma\Delta}} &= \begin{bmatrix} \mathbf{I^{\Sigma}} \\ \mathbf{I^{\Delta}} \end{bmatrix} \in \mathbb{R}^{2m} \\ A_{\Sigma\Delta} &= \begin{bmatrix} -L_{\Sigma}^{-1}R_{\Sigma} & \mathbb{O}_m \\ \mathbb{O}_m & -L_{\Delta}^{-1}R_{\Delta} \end{bmatrix} \in \mathcal{M}_{2m}(\mathbb{R}) \\ B_{\Sigma\Delta} &= -\begin{bmatrix} L_{\Sigma}^{-1} & L_{\Sigma}^{-1} \\ L_{\Delta}^{-1} & -L_{\Delta}^{-1} \end{bmatrix} \in \mathcal{M}_{2m}(\mathbb{R}) \\ \mathbf{E_{\Sigma\Delta}} &= \begin{bmatrix} L_{\Sigma}^{-1}\ \left[\left(v_x^{\Sigma} + 2v_{NO}\right)\mathbf{n_{\Sigma}} - 2\mathbf{V_y}\right] \\ L_{\Delta}^{-1}\ \left[v_x^{\Delta}\mathbf{n_{\Sigma}}\right] \end{bmatrix} \in \mathbb{R}^{2m} \end{aligned} \tag{10}$$

and $R_{\Sigma} = (R+2R_o)\mathbb{I}_m + R_s\mathbb{J}_m$, $L_{\Sigma} = (L+2L_o)\mathbb{I}_m + L_s\mathbb{J}_m$, $R_{\Delta} = R\mathbb{I}_m + R_s\mathbb{J}_m$ and $L_{\Delta} = L\mathbb{I}_m + L_s\mathbb{J}_m$. Equations (9)-(10) apply to any number m of phases.

C. Model of the arm energies

Computing the power flowing through an arm is the first step towards developing the arm energy model. Taking advantage of the current state-space model (9), where $B_{\Sigma\Delta}$ is invertible, $\mathbf{V_{xy}}$ becomes:

$$\mathbf{V_{xy}} = B_{\Sigma\Delta}^{-1}\left(\dot{\mathbf{I}}^{\mathbf{\Sigma\Delta}} - A_{\Sigma\Delta}\mathbf{I^{\Sigma\Delta}} - \mathbf{E_{\Sigma\Delta}}\right) \tag{11}$$

Let $p_y \triangleq p_{py} + p_{ny} = v_{py}\ i_{py} + v_{ny}\ i_{ny}$ be the power flowing through a leg $\#y$ of the converter. Knowing the relationship defining $\{i_{xy}^{\Sigma}; i_{xy}^{\Delta}\}$ from $\{i_{py}; i_{ny}\}$ as given in Table I, one has $p_y = \frac{1}{2}\left(v_{py}\left(i_{xy}^{\Sigma} + i_{xy}^{\Delta}\right) + v_{ny}\left(i_{xy}^{\Sigma} - i_{xy}^{\Delta}\right)\right)$. Thus, the vector $\mathbf{P} = [p_{y_1} \ldots p_{y_m}]^T$ is equal to:

$$\mathbf{P} = \begin{bmatrix} \mathbb{I}_m & \mathbb{I}_m \end{bmatrix} \mathbf{V_{xy}} \circ \frac{1}{2}\begin{bmatrix} \mathbb{I}_m & \mathbb{I}_m \\ \mathbb{I}_m & -\mathbb{I}_m \end{bmatrix} \mathbf{I^{\Sigma\Delta}} \tag{12}$$

where $\circ$ is the HADAMARD or element-wise matrix product. Substituting $\mathbf{V_{xy}}$ in (12) with its expression from (11), $\mathbf{P}$ can be written as a function of the currents only. Assuming that the MMC operates around a nominal DC bus voltage and that DC and AC neutral points share the same voltage, $v_x^{\Delta} = V_{DC}$, $v_x^{\Sigma} = 0$ and $v_{NO} = 0$. Thus, $\mathbf{P}$ can be simplified. Let $\mathbf{E} = [E_{y_1} \ldots E_{y_m}]^T$ be the vector containing the energies of each leg. The dynamic model for $\mathbf{E}$ is simply $\dot{\mathbf{E}} = \mathbf{P}$, or:

$$\dot{\mathbf{E}} = \mathbf{P} = \left[\frac{V_{DC}}{2} - \frac{Z_{\Delta}}{2}\ \mathbf{I^{\Delta}}\right] \circ \mathbf{I^{\Delta}} - \left[\mathbf{V_y} - \frac{Z_{\Sigma}}{2}\ \mathbf{I^{\Sigma}}\right] \circ \mathbf{I^{\Sigma}} \tag{13}$$

where $Z_{\Sigma} = R_{\Sigma} + L_{\Sigma}s$ and $Z_{\Delta} = R_{\Delta} + L_{\Delta}s$.

D. Model of the voltages

Here and for the simulations presented in Section IV, half-bridge submodules (SM-HB) are considered. However, the proposed control architecture can be extended to other submodule types. Applying KIRCHHOFF's and OHM's laws to any SM-HB $\#xyj$ gives the following *average value model*:

$$\begin{cases} i_{C_{xyj}} = D_{xyj}\ \sigma(x)\ i_{xy} = C\ \dot{v}_{C_{xyj}} \\ v_{xyj} = D_{xyj}\ v_{C_{xyj}} \end{cases} \tag{14}$$

where $i_{C_{xyj}}$ and $v_{C_{xyj}}$ are the capacitor current and voltage, $D_{xyj} \in [0;1]$ is the duty cycle of the cell, v_{xyj} is the voltage across the terminals of the cell and, $\sigma(x) = 1$ for $x = p$ and $\sigma(x) = -1$ for $x = n$. A discrete-time vector model is deduced that describes the behavior of all the SM capacitors in an arm:

$$\frac{\mathbf{V_{C_{xy}}}(k+1) - \mathbf{V_{C_{xy}}}(k)}{T_c} = \frac{\sigma(x)\ i_{xy}}{C}\begin{bmatrix} D_{xy1} \\ \vdots \\ D_{xyN} \end{bmatrix} = \frac{\sigma(x)\ i_{xy}}{C}\mathbf{D_{xy}} \tag{15}$$

where T_c is the control sampling period and $\mathbf{V_{C_{xy}}} = [v_{C_{xy1}} \ldots v_{C_{xyN}}]^T \in \mathbb{R}^N$. According to Fig. 1, each arm voltage is made of the series connection of N SMs. Thus,

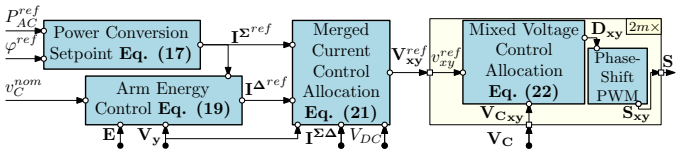

Fig. 2. Proposed control allocation architecture for the MMC

KVL applied to any arm of the converter gives $v_{xy} = \sum_j v_{xyj}$. Using the expression of v_{xyj} in (14), it follows that:

$$v_{xy} = {\mathbf{V_{C_{xy}}}}^T \, \mathbf{D_{xy}} \tag{16}$$

III. Control allocation of the MMC

A. Control architecture of the MMC

The novel control architecture of the MMC proposed in this paper is shown in Fig. 2 and is made of three cascaded loops: a first one for power and energy control, a second one for current reference tracking, and a third one dedicated to the control of the arm and capacitor voltages. Each loop is detailed in the following subsections.

B. Arm energy control and power conversion setpoint

From the specification of a power reference to convert from DC to AC, the $\mathbf{I^{\Sigma}}^{ref}$ current reference is computed. The average AC power is defined by $P_{AC} = \frac{m}{2}\hat{V}_{AC}\hat{I}_{AC}\cos(\varphi)$. Thus, the AC current reference amplitude in phase $\#y$ is deduced. With a null common mode current reference, $i_{xy}^{\Sigma\ ref}$ becomes:

$$\forall y \in \{y_1..y_m\}, i_{xy}^{\Sigma^{ref}} = \frac{2\ P_{AC}^{ref}}{m\hat{V}_{AC}\cos(\varphi^{ref})}\sin\left(\omega_o t - \varphi_y - \varphi^{ref}\right) \tag{17}$$

where $\varphi_{y_k} = (k-1)\ 2\pi/m$. To ensure the tracking of the arm energy reference, an MIB control allocation is implemented. To do so, the MMC power balance model (13) is inverted. Neglecting the losses due to $\mathbf{I^{\Delta}}$, (13) becomes:

$$\dot{\mathbf{E}} = \frac{V_{DC}}{2}\ \mathbf{I^{\Delta}} - \left[\mathbf{V_y} + \frac{Z_\Sigma}{2}\ \mathbf{I^{\Sigma}}\right] \circ \mathbf{I^{\Sigma}} \tag{18}$$

Let $\dot{\mathbf{E}}^* = A_M^E\mathbf{E} + B_M^E\mathbf{E}^{ref}$ be the arm energies reference model (RM), with $\mathbf{E}^{ref} = N\ C/2\ {v_C^{nom}}^2\ \cdot\ [1\dots1]^T \in \mathbb{R}^m$. The RM is chosen to be stable and to represent desirable closed-loop dynamics of the arm energy control loop. To ensure that this behavior is obtained with $\mathbf{I^{\Sigma}}^{ref}$ already determined by (17), the only remaining degree of freedom is the current vector $\mathbf{I^{\Delta}}^{ref}$. The vector is chosen so that $\dot{\mathbf{E}}^* = \dot{\mathbf{E}}$:

$$\mathbf{I^{\Delta}}^{ref} = \frac{2}{V_{DC}}\left(\left[A_M^E\mathbf{E} + B_M^E\mathbf{E}^{ref}\right] + \left[\mathbf{V_y} + \frac{Z_\Sigma}{2}\ \mathbf{I^{\Sigma}}^{ref}\right] \circ \mathbf{I^{\Sigma}}^{ref}\right) \tag{19}$$

C. Current CA

Let $\dot{\mathbf{I}}^{\mathbf{\Sigma\Delta}*} = A_M^I\mathbf{I^{\Sigma\Delta}} + B_M^I\mathbf{I^{\Sigma\Delta}}^{ref}$, with $\mathbf{I^{\Sigma\Delta}}^{ref} = [\mathbf{I^{\Sigma}}^{ref}\ \ \mathbf{I^{\Delta}}^{ref}]^T$, be the current RM. To ensure that this dynamic behavior is reached, the voltage vector $\mathbf{V_{xy}^{ref}}$ must impose $\dot{\mathbf{I}}^{\mathbf{\Sigma\Delta}*} = \dot{\mathbf{I}}^{\mathbf{\Sigma\Delta}}$. According to (9), the condition is equivalent to:

$$B_{\Sigma\Delta}\mathbf{V_{xy}^{ref}} = \dot{\mathbf{I}}^{\mathbf{\Sigma\Delta}*} - A_{\Sigma\Delta}\mathbf{I^{\Sigma\Delta}} - \mathbf{E_{\Sigma\Delta}} \tag{20}$$

This equation takes the usual form of the CA, $M\mathbf{U} = \mathbf{a_d}$, with M the control effectiveness matrix, $\mathbf{U}$ the control vector to be determined, and $\mathbf{a_d}$ the desired action vector [11], [19], [23], [24]. In this case, $M = B_{\Sigma\Delta}$ is invertible, so that a MIB-CA without taking control saturations into account is simply: $\mathbf{U} = M^{-1}\ \mathbf{a_d}$. The control vector $\mathbf{V_{xy}^{ref}}$ is therefore calculated directly as:

$$\mathbf{V_{xy}^{ref}} = B_{\Sigma\Delta}^{-1}\left(\left[A_M^I\mathbf{I^{\Sigma\Delta}} + B_M^I\mathbf{I^{\Sigma\Delta}}^{ref}\right] - \left[A_{\Sigma\Delta}\mathbf{I^{\Sigma\Delta}} + \mathbf{E_{\Sigma\Delta}}\right]\right) \tag{21}$$

In the presence of a static error on the current reference tracking, integral action can be added to the CA, as proposed in [19].

D. Mixed CA of arm and capacitor voltages

Each arm has its own voltage controller which makes a total of $2m$ voltage controllers. Unlike traditionnal MMC voltage control methods, the objectives of arm voltage reference tracking and of capacitor voltage balancing are dealt with simultaneously and in a cooperative fashion in the proposed approach.

The primary voltage control objective is to guarantee that the arm voltage reference computed by the current control algorithm is met. However, the same control actions must also balance the capacitor voltages. The additional requirement is treated as a secondary objective and combined in a joint optimization criterion. In the criterion, the primary objective is to minimize the difference between v_{xy} and v_{xy}^{ref}. The secondary objective is formulated as minimizing the difference between the capacitor voltages $\mathbf{V_{C_{xy}}}$ and $\langle\mathbf{V_{C_{xy}}}\rangle$, the average of the capacitor voltages in the same arm at the current time step. Duty cycle limits lead to the constrained optimization problem:

$$\begin{aligned}&\text{Optimization to solve for each of the } 2m \text{ arms:}\\ &\min_{\mathbf{D_{xy}}} J = \tfrac{1}{N}\left|\mathbf{V_{C_{xy}}}^T\mathbf{D_{xy}} - v_{xy}^{ref}\right| + \mathbf{w} \circ \left|\mathbf{D_{xy}} - \mathbf{D_{xy}^{pref}}\right|\\ &\text{subject to: } \mathbf{D_{min}} \le \mathbf{D_{xy}} \le \mathbf{D_{max}}\end{aligned} \tag{22}$$

The formulation of primary and secondary objectives are deduced from (16) and (15), respectively. $\mathbf{D_{xy}^{pref}}$ is the preferred value of the control vector. The concept of balancing is interpreted as the goal of steering the capacitor voltages towards their average at the next time step. Considering (15), it follows that: $\mathbf{D_{xy}^{pref}} = \frac{C}{T_c\sigma(x)i_{xy}}\left(\langle\mathbf{V_{C_{xy}}}\rangle - \mathbf{V_{C_{xy}}}\right)$. The factor $1/N$ was applied to the primary objective so that the two criteria have comparable orders of magnitude regardless of N.

Note that the system is overactuated when considering the primary objective alone, and underactuated when considering both objectives. Even though the first goal is to track the arm voltage reference, capacitor balancing is also important, even

if it is secondary and cannot be achieved exactly, in general. Thus, the weighting vector $\mathbf{w} = \left|\langle \mathbf{V_{C_{xy}}} \rangle - \mathbf{V_{C_{xy}}}\right| / \langle \mathbf{V_{C_{xy}}} \rangle$ is carefully selected to give a higher priority to restoring capacitor voltages that are far from the average value.

In nominal operation, duty cycles should remain within the range from 0 to 1: $\mathbf{D_{min}} = [0 \dots 0]^T$ and $\mathbf{D_{max}} = [1 \dots 1]^T$. However, as soon as an SM is determined to be faulty, it is shunted by a dedicated *bypass switch*, see Fig. 1 from [25]. The action is taken into account in the optimization algorithm (22) by replacing 1 with 0 for the corresponding components of $\mathbf{D_{max}}$.

The optimization problem (22) can be solved in real-time at every sampling instant using a linear-programming (LP) simplex algorithm designed to solve control allocation problems [11]. The voltage control thus calls for an error-minimization online (EMOn) CA. The optimal duty cycles are computed for each arm and are converted into SM switching states $\mathbf{S_{xy}}$ using the same PWM technique for all $2m$ arms. In each arm, the N carriers are shifted by $2\pi/N$.

IV. Control Simulation and Testing

A. Test procedure

To verify that the control allocation architecture proposed here is capable of achieving the objectives for which it was designed, tests are carried out in simulations. Five different behaviors are tested: 1) progressive power ramp-up, 2) healthy steady-state behavior, 3) healthy transient behavior, 4) steady-state behavior under SM faults, and 5) transient behavior under SM faults. The setpoint power profile shown on Fig. 3 was designed to trigger sequentially all five behaviors as highligthed at the bottom of the figure. The control architecture from Fig. 2 is also fed by two other signals: $\varphi^{ref} = 16.7°$ and $v_C^{nom} = 1.6$ kV which remain at the same values over the entire simulation. $\varphi^{ref} = 16.7°$ is chosen so that $Q_{AC} = 30\% P_{AC}$, in order to assess the control of the MMC on an operating point where the reactive power is non zero. Table II gives the parameters of the MMC[1], of the simulation, and of the reference model. To evaluate the fault tolerant capabilities of the control algorithm, the shunt of 5 SMs out of 50 (i.e. 10% of the SMs) is engaged at $t = 5$ s in arm $\#py_1$. The shunt of the SMs is detected by the control algorithm one sampling step later. To validate the balancing capabilities of the algorithm, the N capacitors of each arm are initialized with a uniform distribution between 75% and 85% of their nominal voltage.

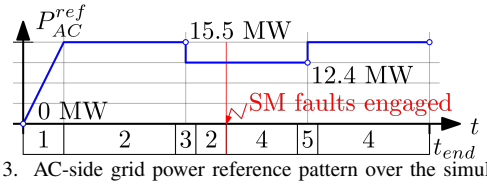

Fig. 3. AC-side grid power reference pattern over the simulation

[1]Note that in the case where no circulating current is injected, this same MMC can provide up to 23.2 MVA to the AC-side grid.

TABLE II
Simulation Parameters of the MMC

Description	Value
MMC rated apparent power	$S_{AC}^{nom} = 16.2$ MVA
DC bus voltage	$V_{DC} = 72$ kV
Half-bus voltages	$v_p = -v_n = V_{DC}/2$
DC bus impedance	$R_s = 0\ \Omega$, $L_s = 0$ H
Arm impedance	R=50 mΩ, L=50 mH
Number of SMs per arm	$N = 50$
SM Capacitor	$C = 10$ mF
Capacitor nominal voltage	$v_C^{nom} = 1.6$ kV
PWM switching period	$T_s = 250$ µs
AC voltage RMS	$V_{AC}^{rms} = 21.6$ kV
AC voltage amplitude	$\hat{V}_{AC} \simeq 30.55$ kV
AC grid frequency and period	f_o=50 Hz, T_o=20 ms
AC-side grid voltage	$v_y = \hat{V}_{AC} \sin(2\pi f_o t - \varphi_y)$
AC-side impedance	R_o=50 mΩ, L_o=50 mH
Simulation time step	$T_{step} = 250$ µs
Simulation duration	$t_{end} = 500 \cdot T_o = 10$ s
Control sampling period	$T_c = T_{step} = 250$ µs
Current RM	$A_M^I \simeq -4712\ \mathbb{I}_{2m}$, $B_M^I = -A_M^I$
Energy RM	$A_M^E \simeq -114\ \mathbb{I}_m$, $B_M^E = -A_M^E$

B. Simulation results and analysis

Figs. 4-10 show the simulation results. As Fig. 4 shows, tracking of the AC grid power setpoint is achieved with a small static error. This static deviation is explained by the presence of a static error in the current reference tracking, barely visible in Fig. 5. Steady state performance can be improved with the introduction of integral action in the current control allocation. [19], [20] has shown how this can be achieved in a transparent manner, meaning that the same RM dynamics are achieved as before the integral action is added. However, such improvement was not judged necessary in the simulations of this paper and was not included.

Considering active capacitor balancing, Fig. 8 shows in red the envelopes of all capacitor voltages and in blue a capacitor voltage randomly chosen among the 300 ones. Over the whole simulation, capacitor balancing is maintained within a ± 2.0 % band around the nominal value as highlighted by Fig. 9. Initialized between 75% and 85% of their nominal value, Fig. 10 show that the capacitor voltages reach their nominal value in about 75 ms, which underlines the quality of the voltage control allocation.

Fig. 6-7 show the quality of the arm voltage reference tracking and the evolution of the associated duty cycles in the $\#py_1$ arm. When the faulty arm loses 5 SMs at $t = 5$ s, the arm voltage reference tracking is lost, but in a single sampling step, the control allocation readily redistributes the control effort optimally so that the arm voltage keeps tracking its reference. As expected, a surge in the duty cyles of the healthy remaining SMs is observed.

About the computational resources needed to run the real-time optimization CA, the simulation computer has an Intel Core i7 with 2.20 GHz frequency and a 16 GB RAM. For $N = 50$, running the LP algorithm takes 30.4 iterations per arm and a total of 340 µs per sampling period on average over the entire simulation.

CONCLUSIONS

A new control approach was proposed for the MMC. First, a control-oriented model of the MMC was derived that described the dynamic behavior of the electrical quantities to be controlled. Then, a multi-loop architecture was developed where the inner core was a novel voltage regulation algorithm using control allocation. The approach made it possible to combine in an optimal and coordinated fashion the objectives of output voltage reference tracking and of capacitor balancing. The procedure takes advantage of each of the multiple submodules in an optimal manner. A useful feature of the methodology is that the dynamics of the closed-loops can be conveniently set using reference models. In the last section, a testing procedure was implemented in simulation. Very good control performance was observed in steady state as well as in transients.

Control allocation methods have found applications in a wide range of air, land, and sea vehicles. This paper pushes a new frontier with power electronic converters requiring much higher sampling frequencies and control variables. A benefit of the CA approach in MMCs is not only that an optimal strategy is obtained for the multiple and conflicting objectives to be achieved, but also that the same algorithm can be used with any number of phases and submodules. Also, the algorithm is able to reconfigure the system for fault-tolerance with almost no changes needed to the control software: when a fault appears, CA immediately reconfigures the use of the SMs, and arm voltage reference tracking is promptly recovered.

The approach of this paper may yield a new generation of resilient MMCs benefiting many electrical power systems, including the integration of renewable sources in the grid.

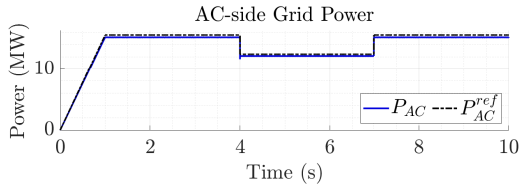

Fig. 4. AC-side grid power reference tracking.

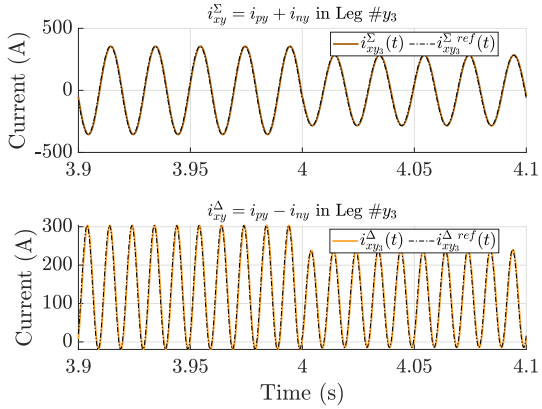

Fig. 5. Current reference tracking, zoom for $t \in [3.9; 4.1]$ s.

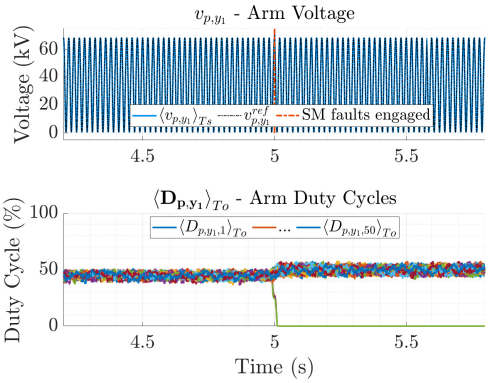

Fig. 6. $\#py_1$ Arm voltage and duty cycles, zoom for $t \in [4.2; 5.8]$ s.

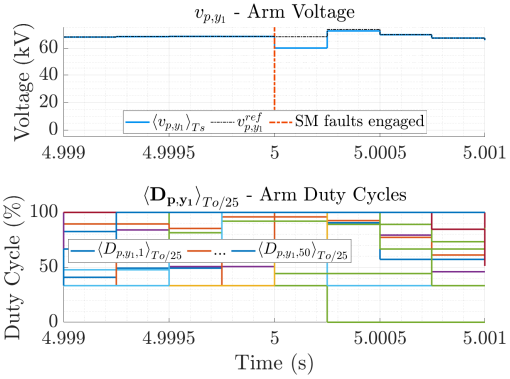

Fig. 7. $\#py_1$ Arm voltage and duty cycles, zoom at the fault engagement time.

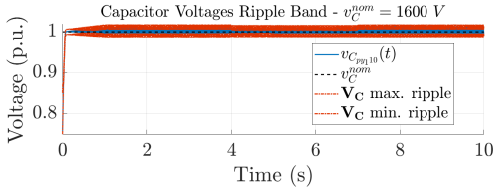

Fig. 8. Ripple band of all capacitor voltages over the entire simulation.

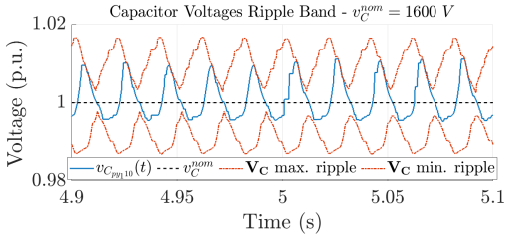

Fig. 9. Zoom of Fig. 8 for $t \in [4.9; 5.1]$ s.

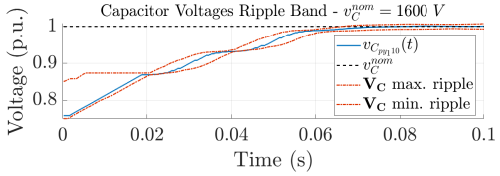

Fig. 10. Zoom of Fig. 8 for $t \in [0; 0.1]$ s.

REFERENCES

[1] "World Energy Outlook 2023 – Analysis," 2023.

[2] M. S. Alam, F. S. Al-Ismail, A. Salem, and M. A. Abido, "High-Level Penetration of Renewable Energy Sources Into Grid Utility: Challenges and Solutions," *IEEE Access*, vol. 8, pp. 190 277–190 299, 2020.

[3] M. A. Perez, S. Ceballos, G. Konstantinou, J. Pou, and R. P. Aguilera, "Modular Multilevel Converters: Recent Achievements and Challenges," *IEEE Open Journal of the Industrial Electronics Society*, vol. 2, pp. 224–239, 2021.

[4] G. Le Goff, M. Fadel, and M. Bodson, "Scalable Optimal Control Allocation: Linear and Quadratic Programming Methods Applied to Active Capacitor Balancing in Modular Multilevel Converters," *IFAC-PapersOnLine*, vol. 55, no. 16, pp. 80–85, Jan. 2022.

[5] ——, "Scalable Control Allocation: Real-time Optimized Current Control in the Modular Multilevel Converter for Polyphase Systems," in *2022 International Symposium on Power Electronics, Electrical Drives, Automation and Motion (SPEEDAM)*, Sorrento, Italy, Jun. 2022, pp. 712–718.

[6] K. Sharifabadi, L. Harnefors, H.-P. Nee, S. Norrga, and R. Teodorescu, "Dynamics and control," in *Design, control, and application of modular multilevel converters for HVDC transmission systems*. Wiley-IEEE Press, 2016, pp. 133–213.

[7] A. Lesnicar and R. Marquardt, "An innovative modular multilevel converter topology suitable for a wide power range," in *2003 IEEE Bologna Power Tech Conference Proceedings*, vol. 3, Jun. 2003.

[8] H. Saad, X. Guillaud, J. Mahseredjian, S. Dennetiere, and S. Nguefeu, "MMC Capacitor Voltage Decoupling and Balancing Controls," *IEEE Transactions on Power Delivery*, vol. 30, no. 2, pp. 704–712, Apr. 2015.

[9] F. J. Lallman, "Relative control effectiveness technique with application to airplane control coordination," Apr. 1985, - NASA Technical Reports Server - Report Number: NAS 1.60:2416.

[10] R. L. Grogan, *On the Application of Neural Network Computing to the Constrained Control Allocation Problem*, ser. Masters' Thesis. Virginia Polytechnic Institute and State University, 1994.

[11] M. Bodson, "Evaluation of optimization methods for control allocation," *Journal of Guidance, Control, and Dynamics*, vol. 25, no. 4, pp. 703–711, Jul. 2002.

[12] B. S. Riar, T. Geyer, and U. K. Madawala, "Model Predictive Direct Current Control of Modular Multilevel Converters: Modeling, Analysis, and Experimental Evaluation," *IEEE Transactions on Power Electronics*, vol. 30, no. 1, pp. 431–439, Jan. 2015.

[13] T. Geyer, "Model Predictive Control of a Modular Multilevel Converter," in *Model Predictive Control of High Power Converters and Industrial Drives*. John Wiley & Sons, Ltd, 2016, pp. 474–504.

[14] P. Hu, D. Jiang, Y. Zhou, Y. Liang, J. Guo, and Z. Lin, "Energy-balancing Control Strategy for Modular Multilevel Converters Under Submodule Fault Conditions," *IEEE Transactions on Power Electronics*, vol. 29, no. 9, pp. 5021–5030, Sep. 2014.

[15] L. Wu, T. Wei, C. Shi, and J. Yin, "Fault-Tolerant Control Strategy for Sub-Module Faults of Modular Multilevel Converters," in *2019 IEEE 12th International Symposium on Diagnostics for Electrical Machines, Power Electronics and Drives (SDEMPED)*, Aug. 2019, pp. 419–424.

[16] D. Zhou, P. Tu, H. Qiu, and Y. Tang, "Finite-Control-Set Model Predictive Control of Modular Multilevel Converters With Cascaded Open-Circuit Fault Ride-Through," *IEEE Journal of Emerging and Selected Topics in Power Electronics*, vol. 8, no. 3, pp. 2943–2953, Sep. 2020.

[17] Q. Xiao, Y. Jin, H. Jia, Y. Tang, A. F. Cupertino, Y. Mu, R. Teodorescu, F. Blaabjerg, and J. Pou, "Review of Fault Diagnosis and Fault-Tolerant Control Methods of the Modular Multilevel Converter Under Submodule Failure," *IEEE Transactions on Power Electronics*, pp. 1–19, 2023.

[18] R. Teodorescu, F. Blaabjerg, M. Liserre, and P. C. Loh, "Proportional-resonant controllers and filters for grid-connected voltage-source converters," *IEE Proceedings - Electric Power Applications*, vol. 153, no. 5, pp. 750–762, Sep. 2006, publisher: IET Digital Library.

[19] G. Le Goff, M. Bodson, and M. Fadel, "Model Reference Control of Constrained Overactuated Systems with Integral Compensation," in *2022 IEEE 61st Conference on Decision and Control (CDC)*, Dec. 2022, pp. 4507–4512.

[20] G. Le Goff, "Scalable Control Allocation Methods for the Modular Multilevel Converter: from Modelling to Real Time Implementation," PhD Thesis, Institut National Polytechnique de Toulouse (INPT), Nov. 2022.

[21] Y. Tian, H. R. Wickramasinghe, Z. Li, J. Pou, and G. Konstantinou, "Review, Classification and Loss Comparison of Modular Multilevel Converter Submodules for HVDC Applications," *Energies*, vol. 15, no. 6, p. 1985, Jan. 2022.

[22] R. Marquardt, "Modular multilevel converters: state of the art and future progress," *IEEE Power Electronics Magazine*, vol. 5, no. 4, pp. 24–31, Dec. 2018.

[23] O. Härkegård, "Backstepping and control allocation with applications to flight control," PhD Thesis, Univ, Linköping, 2003.

[24] A. Bouarfa, M. Fadel, M. Bodson, and J. Lin, "A new control allocation method for power converters and its application to the four-leg two-level inverter," in *2015 23rd Mediterranean Conference on Control and Automation (MED)*, Jun. 2015, pp. 1020–1026.

[25] F. Deng, Y. Tian, R. Zhu, and Z. Chen, "Fault-Tolerant Approach for Modular Multilevel Converters Under Submodule Faults," *IEEE Transactions on Industrial Electronics*, vol. 63, no. 11, pp. 7253–7263, Nov. 2016.